Journal of Materials Chemistry B

ROYAL SOCIETY OF CHEMISTRY

PAPER

View Article Online
View Journal | View Issue

Cite this: J. Mater. Chem. B, 2020, 8, 9362

Bionic intelligent soft actuators: high-strength gradient intelligent hydrogels with diverse controllable deformations and movements†

Qian Zhao, [a] Yanjiao Chang,[a] Zhenglei Yu,[a] Yunhong Liang, *[a] Lei Ren*[b] and Luquan Ren[a]

Received 10th August 2020,
Accepted 16th September 2020

DOI: 10.1039/d0tb01927e

rsc.li/materials-b

A series of novel nanofibrillated cellulose (NFC) reinforced gradient intelligent hydrogels with high response rate, multiple response patterns and diversified self-driven functions were successfully prepared. Based on the effect of the hydroxide radical of NFC on the addition reaction, and on the dehydration synthesis, the variation of NFC significantly regulated the gradient structure of the intelligent hydrogels. In addition to the infiltration property of graphene oxide (GO), reinforcement of NFC enhanced the crosslinking density and Young's modulus, which built a relationship between material characteristics and near infrared laser response rate. Intelligent hydrogel actuators realized bending deformation, curling deformation, switching movements and obstacle avoidance movements. The hydrogels with high Young's modulus exhibited relatively low self-driven rates and efficiency. The self-driven mechanisms of NFC reinforced gradient intelligent hydrogels were revealed effectively by constructing the mathematical relationship curvature variation, bending degree, deformation displacement, material characteristics and incentive intensity. The investigation showed a new path for the combination of mechanical property, intelligent property and functional property of intelligent hydrogels in a bionic soft robot and health engineering.

Introduction

With the development of technology and society, intelligentialize has been the development tendency and forward position field of engineering technology. Under the stimulation of force, temperature, light, electricity and so on, the intelligent soft materials with a low Young's modulus can output relatively high mechanical responses,[1,2] which possess the properties of perception, retroaction and response.[3,4] Compared with traditional rigid materials with a relatively low and simple deformation property, the intelligent soft materials can easily change their shape and adapt to constantly changing circumstances. The properties of elasticity, load capacity,[5,6] human compatibility,[7] low cost[8] and small size, enrich the practical applications of intelligent soft materials in artificial muscle,[9] cytoskeleton,[10] micromanipulator,[11] actuators,[12] soft robots,[13,14] and so on. However, broader applications require that intelligent soft materials should satisfy more complex demands including high load capacity, durability, reusability, stimulation sensibility and stimulation diversification. In addition to excellent mechanical strength, response rate and multivariant deformation, intelligent soft materials should also have authentic perception, response and environmental interaction.[15] Therefore, how to combine the mechanical property, intelligent property and functional property is the bottleneck of intelligent hydrogel design and preparation.

Compared with electrorheological fluids,[16] magnetorheological fluids,[17] dielectric elastomers,[18] liquid-crystal polymers[19] and shape memory polymers,[20] intelligent hydrogels possess abundant stimulation responses and linear driving force output, which provide low cost material selection and efficient operability for practical applications of soft actuators, electron devices and medical appliances.[21–23] The relatively low Young's modulus of the intelligent hydrogels acts as the material base for a high degree of deformation and multiple degree of freedom deformations. Moreover, the disadvantage of mechanical strength of intelligent hydrogels can be improved by material and structure design. As one of the typical intelligent soft materials, intelligent hydrogels face similar bottleneck problems. From the point of view of synthesis method,[24,25] response pattern,[24,26–28] moulding technology[29,30] and mechanical

[a] The Key Laboratory of Bionic Engineering, Ministry of Education, Jilin University, Changchun 130025, China. E-mail: liangyunhong@jlu.edu.cn
[b] School of Mechanical, Aerospace and Civil Engineering, University of Manchester, Manchester, M13 9PL, UK. E-mail: lei.ren@manchester.ac.uk

† Electronic supplementary information (ESI) available. See DOI: 10.1039/d0tb01927e

performance improvement,[31,32] much research has been conducted to realize the high mechanical strength, multiple intelligent responses, high response rate, multiple deformation patterns and efficient self-driven deformation and movement. Even though many suggestions from research have been adopted, many inadequacies still need to be improved. Firstly, from the point of view of the synthesis methods, the adoption of physical crosslinking and chemical crosslinking focused on the change of crosslinking method and improvement of material composition, which failed to improve the mechanical strength of chemical crosslinked hydrogels. The effect of structural factors on mechanical properties and functional properties should be considered to enhance the response rate and mechanical strength. Secondly, even though 3D printing technology was used to enhance the sample dimension precision and response rate of intelligent hydrogel actuators, the realized functional properties of complex deformation pattern and effective locomotion were relatively limited. Because of the relative low deformation degree and response rate, the intelligent hydrogel actuators failed to realize efficient self-driven deformation and locomotion. Thirdly, much research neglected the analysis of self-driven deformation and locomotion mechanisms from the point view of mathematics and mechanics. Therefore, these shortcomings are the development and application bottlenecks of intelligent hydrogels, which need to be solved *via* further research.

In a previous study,[33] a series of near-infrared (NIR) laser-driven intelligent gradient hydrogels with multiple degrees of freedom and a high response rate of 187.7° s^{-1} were successfully prepared using entirety infiltration and locality infiltration of GO. Under the stimulation of NIR, the hydrogels can be used to prepare intelligent actuators including bionic hands, bionic chrysanthemums and bionic inchworms, which exhibited high intelligence and functional properties. The design and preparation of bionic intelligent hydrogel actuators provided a new candidate material for the solving bottleneck problems of producing intelligent soft materials. Even though the prepared gradient intelligent hydrogel had excellent material properties, the disadvantage of a low Young's modulus restricted the further application of gradient hydrogels. Therefore, how to enhance the mechanical properties became the key point of solving the bottleneck problems of production of intelligent gradient hydrogels. As a type of effective mechanical strength reinforcements, nanofibrillated cellulose (NFC) has been used to improve Young's modulus of hydrogels *via* the enhancement of the crosslinking density.[34,35] The NFC was used to build the material base of the gradient intelligent hydrogels because of its mechanical property.

Facing the combination of mechanical strength, response rate and multivariant deformations of intelligent soft materials, gradient intelligent hydrogels prepared *via* hydrothermal synthesis were treated as a basic material base to solve the problem of combining mechanical properties, intelligence properties and functional properties. In this research, by regulating the reinforcement content of NFC, the material and mechanical characteristics of gradient intelligent hydrogels were investigated. Based on infiltration methods of GO and stimulation of NIR, a series of bionic hydrogel actuators with abundant deformations and movements were prepared. Moreover, the self-driven mechanisms were explained *via* mathematics and mechanical analysis, providing a new bionic method for solving bottleneck problems of intelligent soft materials.

Results and discussion

Microstructure of NFC reinforced gradient hydrogels

The addition of NFC into the gradient structure of intelligent hydrogel systems can be successfully used to prepare the NFC reinforced gradient hydrogels *via* hydrothermal synthesis, as shown in Fig. S1 (ESI†). The unbroken macroscopic morphology and decrease of thickness indicated the effective reinforcement role of NFC. The microstructure characteristics of hydrogels before and after entire infiltration of GO further revealed the effect of the NFC content on structure and infiltration properties. Attributed to micropore size scale from top to bottom, the NFC0 gradient intelligent hydrogel was qualitatively divided into four layers (Layer 1, Layer 2, Layer 3 and Layer 4). The micropore size decreased gradually from Layer 1 to Layer 4, as shown in Fig. S2(a-1)–(a-4), ESI,† respectively. After entire infiltration, the GO particles bonded tightly on the smooth micropore surfaces, as shown in Fig. 1(a-1)–(a-4). Because of the entire infiltration characteristic, GO infiltrated into the hydrogel matrix from the periphery to the interior, which led to a relative low amount of GO in Layer 2 and Layer 3. The largest micropore size of Layer 1 exhibited the highest infiltration amount of GO. The densest microstructure of Layer 4 had the least amount of GO.

The addition of NFC changed the gradient microstructure characteristics of NFC0 hydrogel, as shown in Fig. S2(b-1) (ESI†). The NFC content of 1 mg mL^{-1} compacted the network structure of Layer 1 in the NFC0 hydrogel. In addition, because of the micropore with a relatively small size on the bottom, the original gradient structure cannot be observed from the point of view of micropore size variation. The NFC1 hydrogel was divided into a bottom part, middle part and top part, as shown in Fig. S2(b-2)–(b-4) (ESI†), respectively. A small amount (1 mg mL^{-1}) of NFC caused a low convex structure on the micropore surfaces and maintained the infiltration property of the NFC1 hydrogels. The GO particles existed in the three parts. From the bottom part to the top part, the amount of infiltration of GO increased gradually, which changed from a "particle pattern" to a "layered drape pattern", as shown in Fig. 1(b-1)–(b-4).

Compared with the NFC1 hydrogel, the NFC2 hydrogel also exhibited an inconspicuous gradient structure. The original gradient structure of NFC0 was weakened further with the increase of NFC content, as shown in Fig. S2(c-1), ESI.† Compared with the NFC1 hydrogel, the distinct convex structure on the micropore surfaces can be observed in the bottom part, middle part and top part (see Fig. S2(c-2)–(c-4), respectively, ESI†). After entire infiltration, GO with a "particle pattern" bonded tightly on surfaces with a convex structure, as shown in Fig. 1(c-2)–(c-4). The large amount of infiltration of GO covered the original convex structure in the top part [Fig. 1(c-4)].

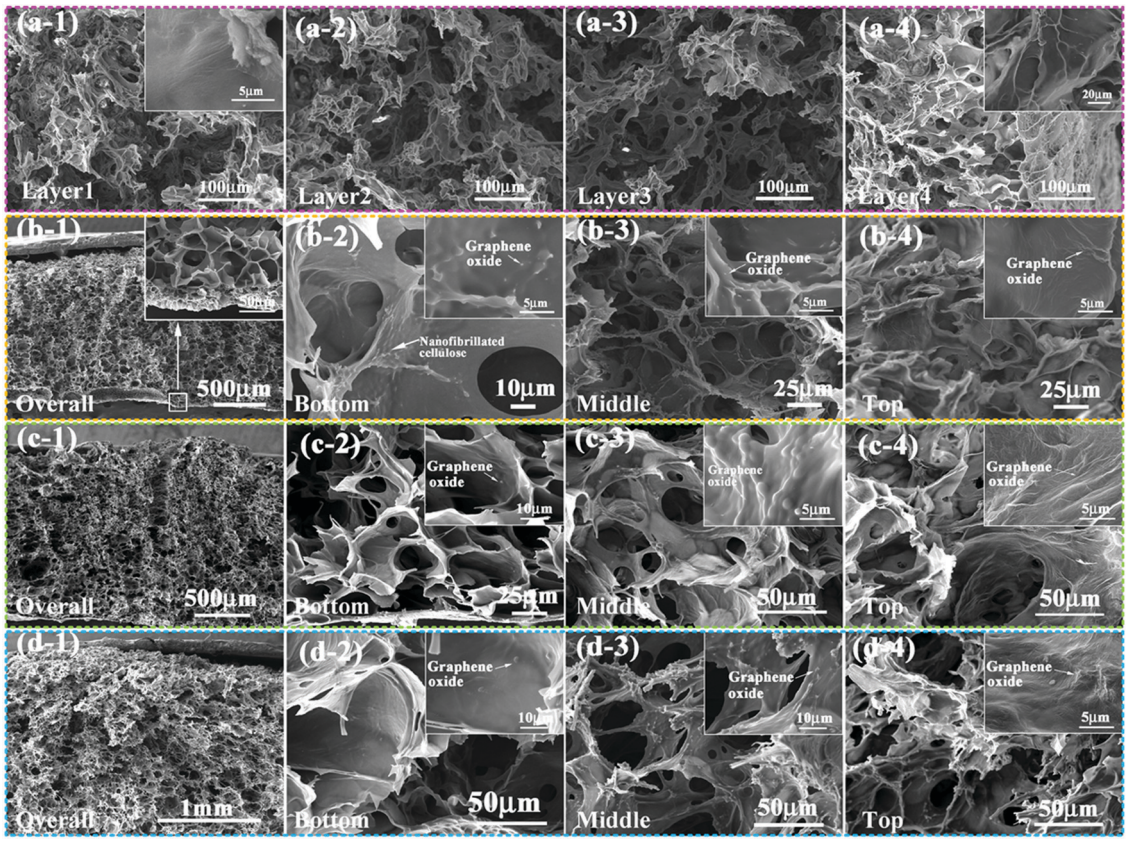

Fig. 1 Microstructure of gradient intelligent hydrogels with different NFC contents after entire infiltration of GO. (a-1)–(a-4) Microstructure of the four layers in NFC0, (b-1)–(b-4) microstructure of the bottom, middle and top parts of NFC1, (c-1)–(c-4) microstructure of the bottom, middle and top parts of NFC2, and (d-1)–(d-4) microstructure of the bottom, middle and top parts of NFC3.

When the NFC content reached 3 mg mL^{-1}, the thickness of the hydrogel decreased further, as shown in Fig. S2(d-1), ESI.† The convex structure induced by the NFC also existed in the bottom, middle and top parts of the NFC3 hydrogel. Compared with the NFC1 and NFC2 hydrogels, the NFC3 hydrogel had a dense and extensive distribution of convex structures, as shown in Fig. S2(d-2)–(d-4), ESI.† After entire infiltration, the NFC3 hydrogel still exhibited a compact structure pattern (see Fig. 1(d-1), ESI†). Moreover, the GO particles showed the ''particle pattern'' and ''layered drape pattern'' in the bottom part (Fig. 1(d-2)), middle part (Fig. 1(d-3)) and top part (Fig. 1(d-4)).

Combining the results from Fig. 1 and Fig. S2 (ESI†), it was found that the variation of the NFC content affected the macrostructure and microstructure. With the increase of NFC content, thickness and gradient structure were decreased and weakened, respectively. The micropore surfaces changed from a smooth structure to a dense convex structure. However, the addition and variation of NFC maintained the GO infiltration property of the hydrogels.

The effect of addition and variation of NFC changed the crosslinking density of the gradient intelligent hydrogels. As shown in Fig. S3 (ESI†), the variation of NFC content maintained the isopropyl and acylamino functional groups. The addition and variation of NFC induced the movement of the peak at 1652 cm^{-1} and maintained the existence of the temperature responsive groups shown in Fig. S4 (ESI†), on which was built the functional base of the NIR response.

In order to evaluate the mechanical property of the NFC reinforced gradient intelligent hydrogels, the Young's moduli obtained from the diagnostic ultrasound imaging apparatus along the direction of the thickness of the hydrogels were analysed, as shown in Fig. S5 (ESI†). Based on the Young's modulus range distribution characteristics, the weak gradient structure and thickness pattern was similar to the microstructure analysis. The maximum of the Young's modulus value of the NFC reinforced gradient intelligent hydrogel was 11.5 kPa for NFC2. The effect of NFC content on Young's modulus showed a turning point of 3 mg mL^{-1}. Fig. S5 (ESI†) showed that the mechanical reinforcement role of NFC was feasible in a gradient intelligent hydrogel system. The optimal reinforcement content of NFC was 2 mg mL^{-1}. The addition of NFC enhanced the mechanical property of the gradient intelligent hydrogels, which were used to build the material base for NIR response rate experiments.

Polymerization mechanisms of an NFC reinforced gradient intelligent hydrogel

Combined with the material compositions and microstructure characteristics of hydrogels, the polymerization mechanisms are shown in Fig. 2. The role of 4-hydroxybutyl acrylate (4HBA)

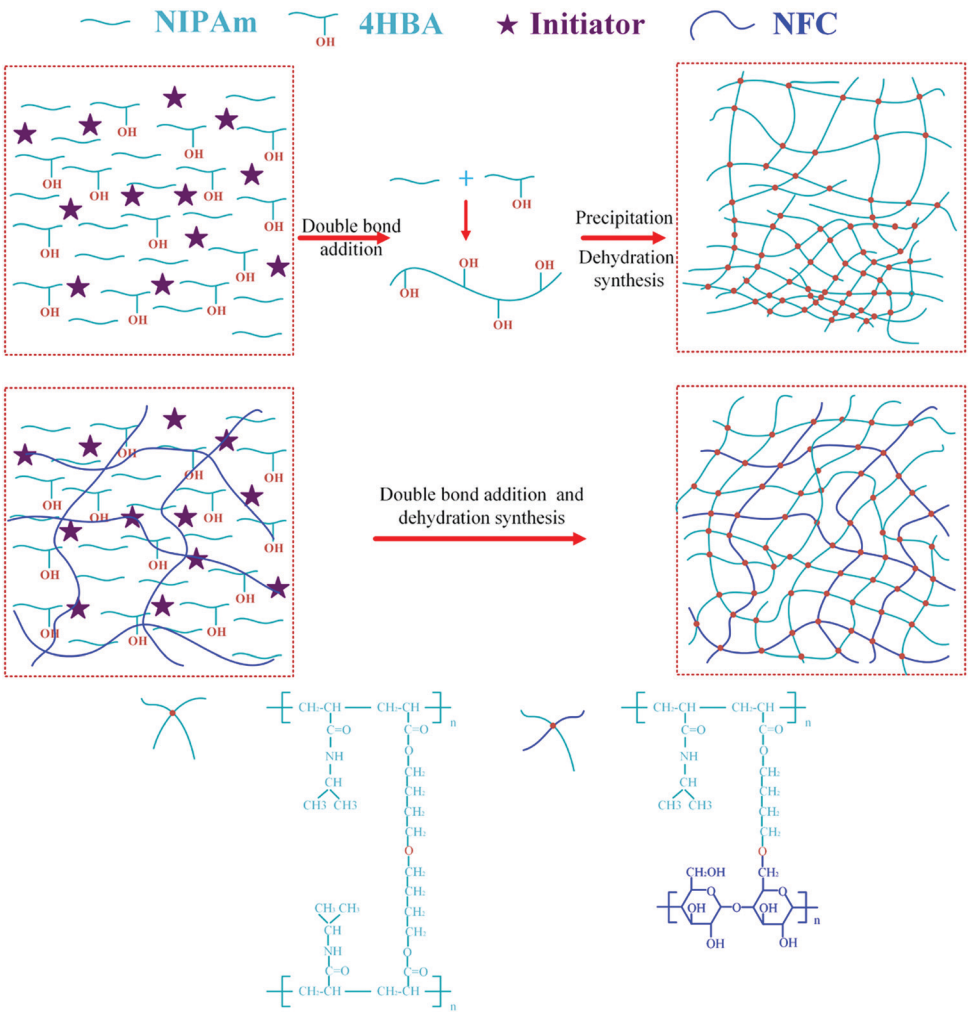

Fig. 2 Polymerization mechanism of nanofibrillated cellulose reinforced gradient intelligent hydrogels.

in a material system without NFC was as a crosslinking agent. In the hydrothermal synthesis between *N*-isopropylacrylamide (NIPAm) and 4HBA, an addition reaction of a double bond led to the existence of a polymer with a hydroxide radical (PNIPAm–4HBA–OH) and ammonium persulfate (APS) was the initiator. The synthesized polymer was precipitated and formed a concentration gradient. In the sedimentation process, dehydration synthesis happened in hydroxide radical of synthesized polymers, forming the gradient network structure.

The 4HBA and non-carboxylated NFC in the material system were crosslinking agents. The long macromolecular chain with a hydroxide radical (PNIPAm–4HBA–OH) was also synthesized by the addition reaction of a double bond in the hydrothermal synthesis between NIPAm and 4HBA. As a type of macromolecule, the dehydration synthesis was a reaction between the long macromolecular chain formed *via* an addition reaction and a hydroxide radical in NFC. At the same time, the dehydration synthesis also occurred between the long macromolecular chains. The NFC dispersed uniformly in water. The dehydration synthesis between NFC and the long macromolecular chains formed by the addition reaction led to a homogeneous network structure of intelligent hydrogels.

As the reinforcement, the NFC enhanced the crosslinking density of hydrogels, which significantly affected the material characteristics of density, moisture content, volume expansion ratio (as shown in Fig. S6, ESI†) and swelling/deswelling rate (see Fig. S7, ESI†). Besides the stable chemical functional groups, the NFC reinforced gradient intelligent hydrogels had high swelling/deswelling rates, which formed the base of intelligence property for NIR-driven hydrogel actuators.

NIR response rate analysis

In order to quantitatively represent the effects of NFC content and NIR power density on the NIR response rate of NFC reinforced intelligent hydrogels, the bending degree was adopted to measure the NIR response rate. Fig. 3(a)–(d) shows the bending degree curves and deformation process of hydrogels under NIR irradiation with different power densities. Because of the low power density, the minimum bending degree of NFC intelligent hydrogels was higher than 90°, as shown in Fig. 3(a). With the increase of NFC content, the minimum bending degree and the time taken to reach the minimum bending degree were decreased and increased, respectively. Before 1.2 s, increasing the NFC content decreased

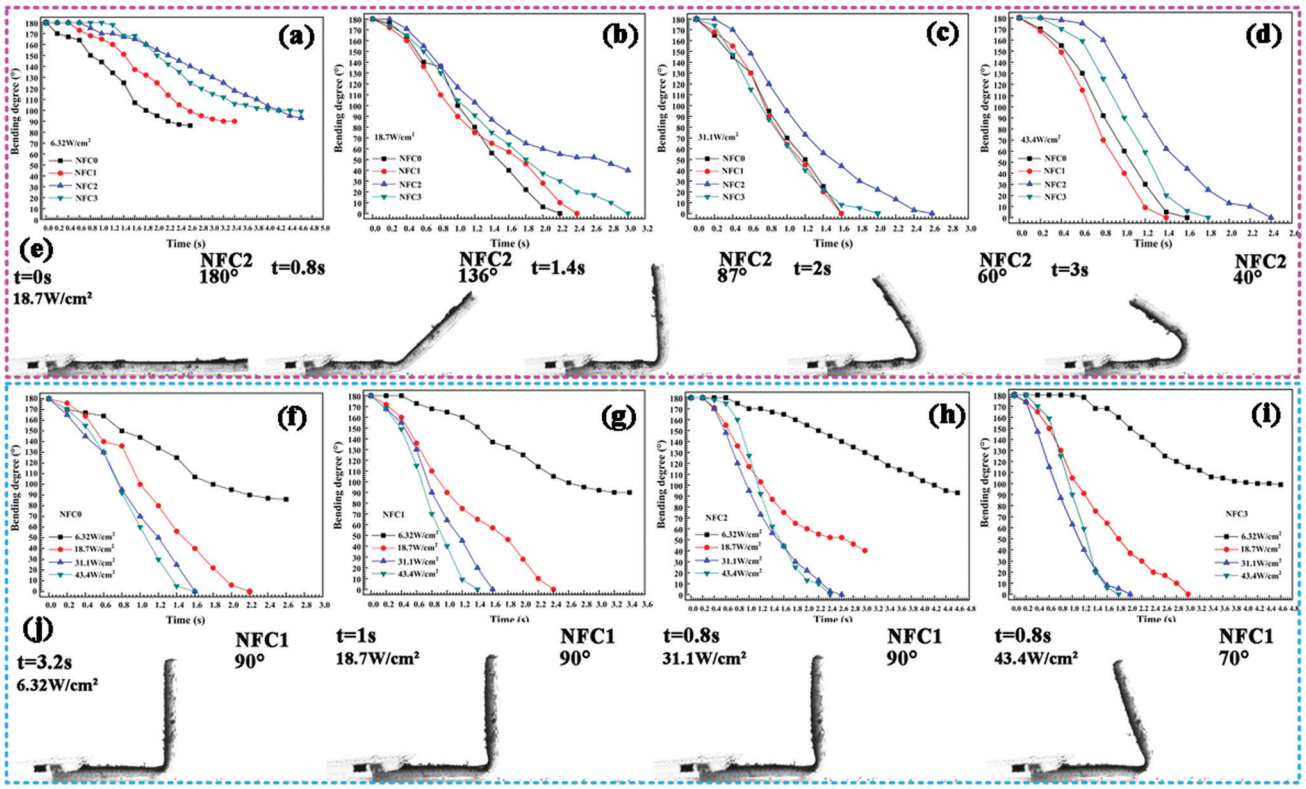

Fig. 3 Effect of laser power densities and NFC contents on bending degree variation of gradient intelligent hydrogels. (a) Power density of 6.32 W cm^{-2}, (b) power density of 18.7 W cm^{-2}, (c) power density of 31.1 W cm^{-2}, (d) power density of 43.4 W cm^{-2}. (e) NIR response process of the NFC2 hydrogel with a power density of 18.7 W cm^{-2}. (f) NFC content of 0 mg mL^{-1}, (g) NFC content of 1 mg mL^{-1}, (h) NFC content of 2 mg mL^{-1}, (i) NFC content of 3 mg mL^{-1} and (j) the time which the NFC1 hydrogels took to reach or be close to 90° bending.

the response rate of the NFC gradient intelligent hydrogels. Compared with the NFC2 hydrogel, the relative low Young's modulus of NFC3 led to a relatively high response rate after 1.6 s. When the laser power density reached 18.7 W cm^{-2}, the minimum bending degrees were lower than 90°, as shown in Fig. 3(b). The minimum bending degree of the NFC2 hydrogel was 40°. Comparing the graphs shown in Fig. 3(b) with those in Fig. 3(a), the increasing power density improved the response rate. The NFC0 intelligent hydrogel took the shortest time to reach a bending degree of 0°. The variation of response rate of intelligent hydrogels with NFC was relevant to the corresponding variation rule of Young's modulus. When the laser power density reached 31.1 W cm^{-2} as seen in Fig. 3(c), the minimum bending degree of the NFC2 hydrogel was 0°. The response rates of the hydrogels were increased further. The highest Young's modulus of the NFC2 hydrogel still showed the lowest response rate. The power density of 31.1 W cm^{-2} weakened the response rate differences of the NFC0, NFC1 and NFC3 hydrogels. Under a power density of 43.4 W cm^{-2}, the NFC reinforced intelligent hydrogels exhibited steady response rate curves, as shown in Fig. 3(d). Combining the results of Fig. 3(b) with those of Fig. S5 (ESI†), the NIR response rate of the NFC reinforced intelligent hydrogels decreased first and then increased, which corresponded to the Young's modulus variation tendency. Even though the Young's modulus of the NFC0 hydrogel was lower than that of the NFC1 hydrogel, the highest moisture content and volume expansion ratio restricted the response rate under the highest laser power density. The NFC2 hydrogel showed the steadiest NIR response process (see Movie S1, ESI†), as shown in results in the pink dotted frame of Fig. 3.

The power density was another important factor for NIR response rate. Fig. 3(e)–(h) show the bending degree curves of NFC reinforced gradient intelligent hydrogels under the irradiation of NIR with different power densities. The response rates of the NFC0 gradient intelligent hydrogel were enhanced with the increase of power density, as shown in Fig. 3(e). Under power densities of 31.1 W cm^{-2} and 43.4 W cm^{-2}, the time for reaching the minimum bending degree of the NFC0 hydrogel was similar. After 1.4–1.6 s, the bending deformation of the NFC0 hydrogel had finished. The volume shrinkage caused by irradiation by NIR was the main deformation pattern (see Movie S2, ESI†). Therefore, the response rate under 43.4 W cm^{-2} was lower than that of 31.1 W cm^{-2} during 1.4–1.6 s. The effect of power density on the response rate of the NFC1 hydrogel was similar to that of the NFC0 hydrogel, as shown in Fig. 3(f). When the NFC content was increased to 2 mg mL^{-1} in Fig. 3(g), the bending degree curve of 43.4 W cm^{-2} shows an unknown process occurs at 0.6 s. After 0.6 s, the response rate increased sharply. As shown in Fig. 3(h), the NFC3 hydrogel also showed an unknown process at 0.2 s under a power density of 43.4 W cm^{-2}. The unknown process

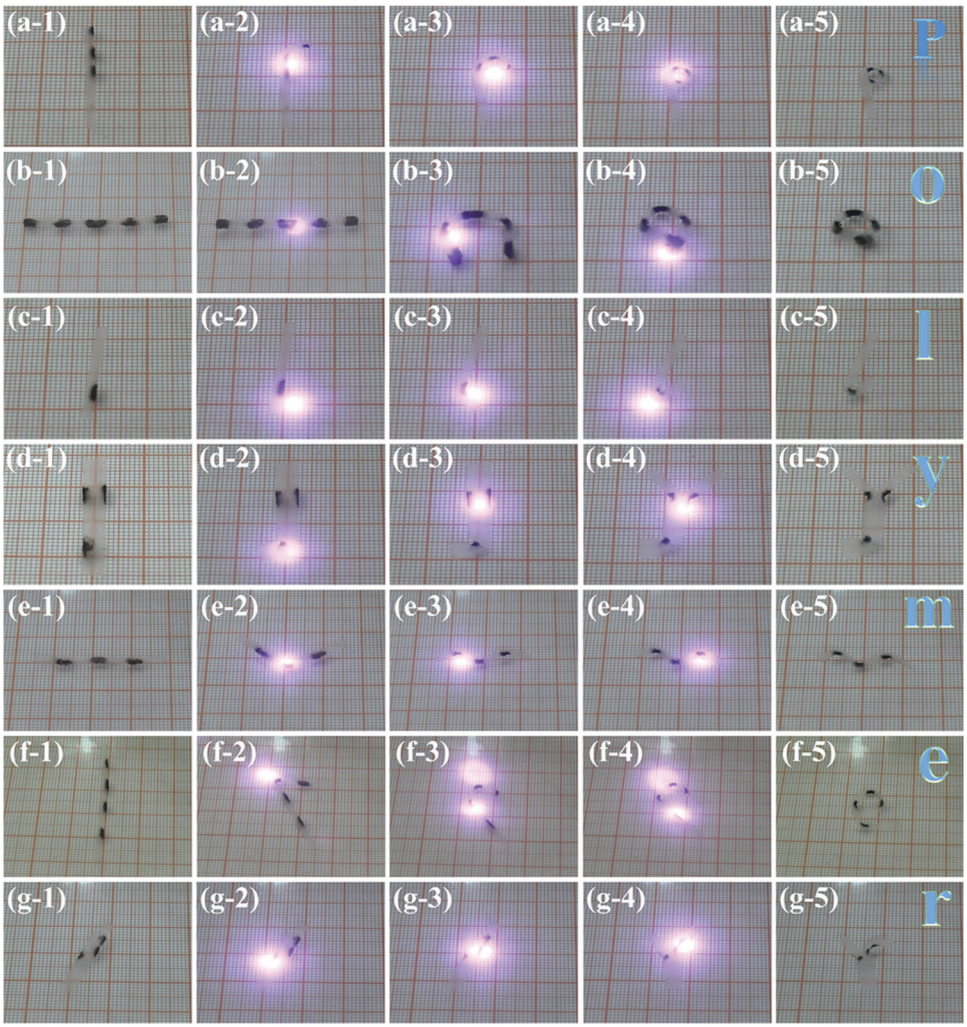

Fig. 4 The deformation process of "Polymer" on the base of the NFC0 gradient intelligent hydrogel. (a-1)–(a-5) Deformation process of "P", (b-1)–(b-5) deformation process of "o", (c-1)–(c-5) deformation process of "l", (d-1)–(d-5) deformation process of "y", (e-1)–(e-5) deformation process of "m", (f-1)–(f-5) deformation process of "e" and (g-1)–(g-5) deformation process of "r".

was found to be a part of the bending process, which was influenced by Young's modulus and power density. Attributed to having the highest Young's modulus, the NFC2 hydrogel exhibited the longest time to reach the minimum bending degree and had a higher resistance to overcome than that of NFC0, NFC1 and NFC3. The unknown process at 6.32 W cm^{-2} resulted from the long time of the photothermal conversion process. The driven force induced by volume shrinkage needed an accumulated process. In this process, the photothermal conversion rates in the top part and the middle part were higher than that in the bottom part, leading to the higher volume shrinkage rates in top part and middle part of the intelligent hydrogels. Bending deformation only existed in the irradiated part. The high power density of 43.4 W cm^{-2} led to volume shrinkage in the top part, middle part and bottom part of the NFC hydrogels. The volume shrinkage rate along the thickness of the hydrogel was higher than the photothermal conversion rates along the length and width. In the irradiated part there existed a volume shrinkage phenomenon. The sufficient volume shrinkage of the top and middle parts along the length and width led to the bending deformation process, which induced the occurrence of the unknown process of the NFC hydrogels at 43.4 W cm^{-2}. The graphs in the blue dotted frame in Fig. 3 show the time to reach or to be closed to 90° of the NFC1 intelligent hydrogel under irradiation of NIR at different power densities. Increasing the power density of the NIR enhanced the response rate of the NFC reinforced gradient intelligent hydrogels, but the excessive power density restricted the increase of response rate. The optimal power density value was found to be 31.1 W cm^{-2}.

By analysing the results shown in Fig. 1–3, it can be seen that the addition of NFC the improved the mechanical strength and enhanced the response rate, which combined the mechanical property and the intelligence property of the intelligent hydrogels. The reinforcement role of NFC in the gradient intelligent hydrogels was feasible, providing an effective method for the design of actuators with diverse controllable deformations and movements *via* infiltration of GO

"Polymer" deformation with intermittent NIR irradiation

The "Polymer" deformation consisted of deformations of the letters: P, o, l, y, m, e and r made out of the intelligent hydrogel, which combined the monodirectional and bidirectional bending property. In order to realize the effective comparable analysis between monodirectional and bidirectional bending deformations, the P of "Polymer" was a capital letter, and the other letters were lowercase. The inflection points of the letters were treated as the locality infiltration positions, as shown in Fig. 4.

Half of the letter "P" had three equidistant infiltration points, as shown in Fig. 4(a-1). The NIR irradiation was used to treat the middle and top infiltration points in sequence, as shown in Fig. 4(a-2) and (a-3), respectively. When the bottom infiltration point was irradiated, the other two points were also covered by NIR, as shown in Fig. 4(a-4). After removing NIR, the NFC0 intelligent hydrogel exhibited the "P" shape as shown in Fig. 4(a-5). The letter "o" had five equidistant infiltration points (see Fig. 4(b-1)). After irradiation of the middle point, the two points near middle point were treated rapidly with NIR irradiation, as shown in Fig. 4(b-2) and (b-3). Next, the two endpoints and the entire sample were subjected to NIR irradiation circularly to give the "o" shape shown in Fig. 4(b-4) and (b-5). The deformation of the letter "l" was relatively simple. Only one infiltration point can give the bending deformation, as shown in Fig. 4(c-1)–(c-5). One third of a hydrogel strip was cut into two parts. Two infiltration points were on the right and left sides of the bifurcation, respectively (see Fig. 4(d-1)). After irradiating the bottom infiltration point, the bifurcation was rapidly subjected to NIR irradiation to give the letter "y" shape, as shown in Fig. 4(d-2)–(d-5). The deformation pattern of the letter "m" was similar to letter "y". The infiltration directions of the right and left points were opposite to the middle one, as shown in Fig. 4(e-1). The middle, left and right points were circularly subjected to NIR irradiation to form the letter "m" shape, as shown in Fig. 4(e-2)–(e-5). Four infiltration points were distributed in the hydrogel strip along the length, as shown in Fig. 4(f-1). Two NIR spots were employed to control the deformation process, as shown in Fig. 4(f-2)–(f-5). Three points were treated as the infiltration positions in Fig. 4(g-1). The left point and right bottom point existed on the bifurcation of the letter "r". After irradiation of the left point, the two points on the right were irradiated to form a letter "r" shape, as shown in Fig. 4(g-2)–(g-5). Based on monodirectional and bidirectional bending property of NFC0 intelligent hydrogels, the combination of "P", "o", "l", "y", "m", "e" and "r" made the word "Polymer". Movie S3 (ESI†) shows the process in detail.

Bionic drosera deformation with intermittent NIR irradiation

In addition to the bending deformation, the NFC reinforced gradient intelligent hydrogels can also show a curling deformation. Inspired by the curling deformation process of the sundew plants (Drosera), a series of bionic drosera hydrogel actuators were prepared. Fig. 5(a-1)–(a-6) show the bionic drosera deformation process of the NFC0 intelligent hydrogel. The sample was subjected to NIR irradiation from the right endpoint to the left endpoint. During the irradiation process, the curled parts

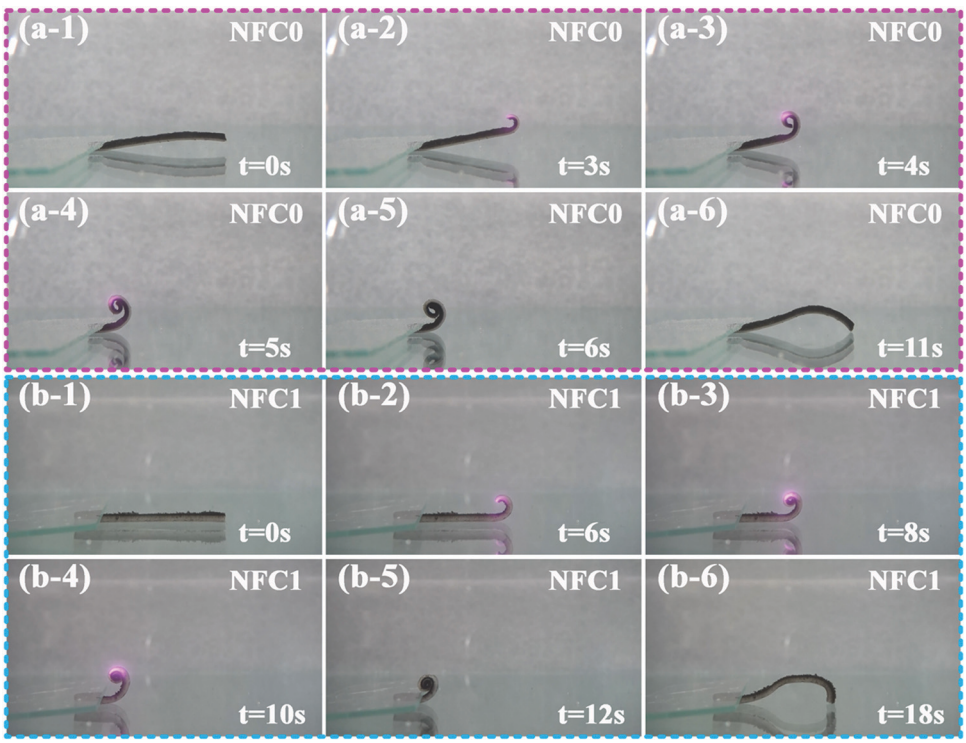

Fig. 5 The bionic drosera deformation processes of gradient intelligent hydrogels with different NFC contents. (a-1)–(a-6) NFC0 hydrogel and (b-1)–(b-6) NFC1 hydrogel.

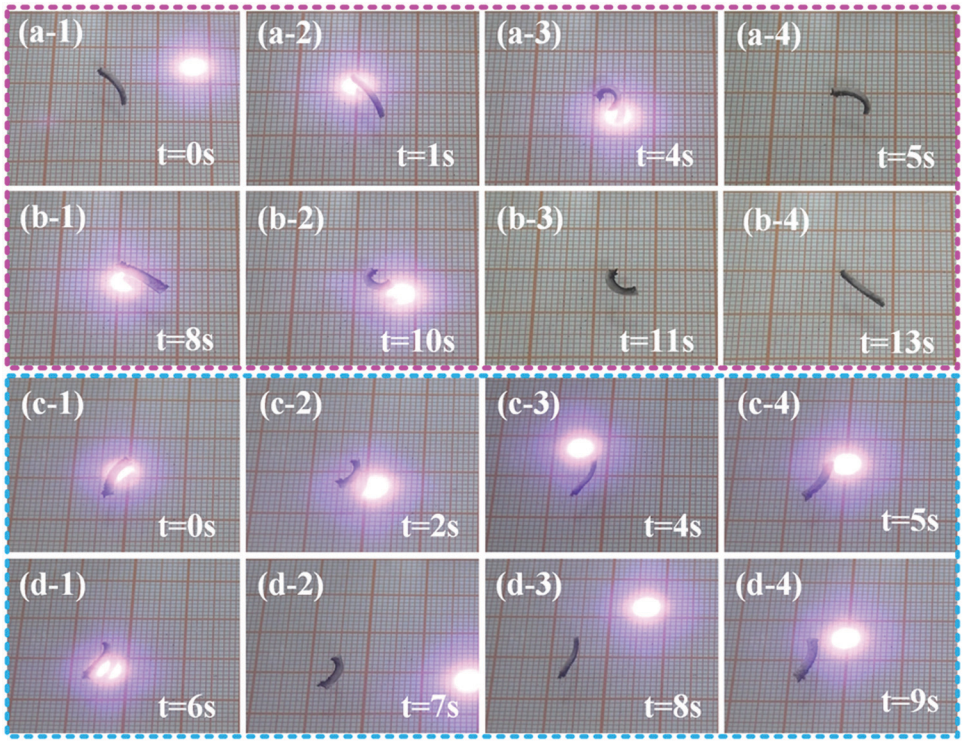

Fig. 6 The 90° circulatory and the homodromous circulatory switching processes of NFC2 gradient intelligent hydrogels. (a-1)–(a-4) Switching 90° to left and (b-1)–(b-4) switching 90° to right with a power density of 6.32 W cm^{-2}. (c-1)–(c-4) The first, and (d-1)–(d-4) the second switching process with a power density of 18.7 W cm^{-2}.

were always under NIR irradiation to maintain the curling deformation. After removing the laser, the curled sample returned to its original state. Compared to the NFC0 hydrogel actuator, the NFC1 sample reached the curled state in 10 s, as shown in Fig. 5(b-1)–(b-4). The time for the hydrogel to recover process 6 s (see Fig. 5(b-5) and (b-6)). As shown in Fig. S8 (ESI†), the NFC2 and NFC3 gradient intelligent hydrogels also showed the bionic drosera deformation. The increase of Young's modulus decreased the curling deformation rate. Because it had the highest Young's modulus, the NFC2 hydrogel actuator took 11 s to reach the curled pattern, as shown in Fig. S8(a-1)–(a-6), ESI.† Moreover, the NFC2 sample exhibited the lowest degree of curling as shown in Fig. S8(a-4), ESI.† Compared with the NFC2 sample, the time taken for the NFC3 hydrogel actuator to reach the curled state was also 11 s, but the final degree of curling was higher than that of NFC2, as shown in Fig. S8(b-1)–(b-6), ESI.† Movie S4 (ESI†) shows the bionic drosera deformation process of NFC reinforced intelligent hydrogels.

Switching movements with intermittent NIR irradiation

Based on the results shown in Fig. 3, power densities of 6.32 W cm^{-2} and 18.7 W cm^{-2} were selected to determine the effect of switching on the movement patterns of NFC2 intelligent hydrogels. Fig. 6(a-1)–(b-4) show two 90° circulatory switching processes of the NFC2 gradient intelligent hydrogel with a power density of 6.32 W cm^{-2}. Fig. 6(a-1) shows the initial state of the NFC2 hydrogel. The sample was treated with NIR irradiation along the length, which induced the volume shrinkage and bending phenomena shown in Fig. 6(a-2) and (a-3). After removing the NIR irradiation, the NFC2 sample switched 90° to left in the unbending process, as shown in Fig. 6(a-4). The final state of the first switching process was treated as the original state of the second switching process. In the unbending process, the NFC2 hydrogel switched 90° to right, as shown in Fig. 6(b-1)–(b-4). The 90° circulatory switching process of the NFC2 hydrogel was reversible and repeatable (see Movie S5, ESI†), which was controlled by the power density and intermittent irradiation pattern.

Fig. 6(c-1)–(d-4) show the homodromous circulatory switching processes of the NFC2 gradient intelligent hydrogel with a power density of 18.7 W cm^{-2}. The NFC2 sample was subjected to NIR irradiation along its length. In the unbending process, the degree of switching shown in Fig. 6(c-1)–(c-4) was larger than the 90° shown in Fig. 6(a-1)–(a-4). Fig. 6(d-1)–(d-4) show the homodromous circulatory switching processes of the NFC2 hydrogel, exhibiting the reversible and repeatable characteristics (see Movie S6, ESI†). It was found that the NIR power density significantly affected the switching characteristics of the NFC2 intelligent hydrogels, which enriched the self-driven functional properties of the NFC reinforced gradient intelligent hydrogels.

Controllable movement with continuous NIR irradiation

In addition to the deformations and movements, the NFC reinforced gradient intelligent hydrogels can show controllable movements with continuous NIR irradiation. Fig. 7(a)–(d)

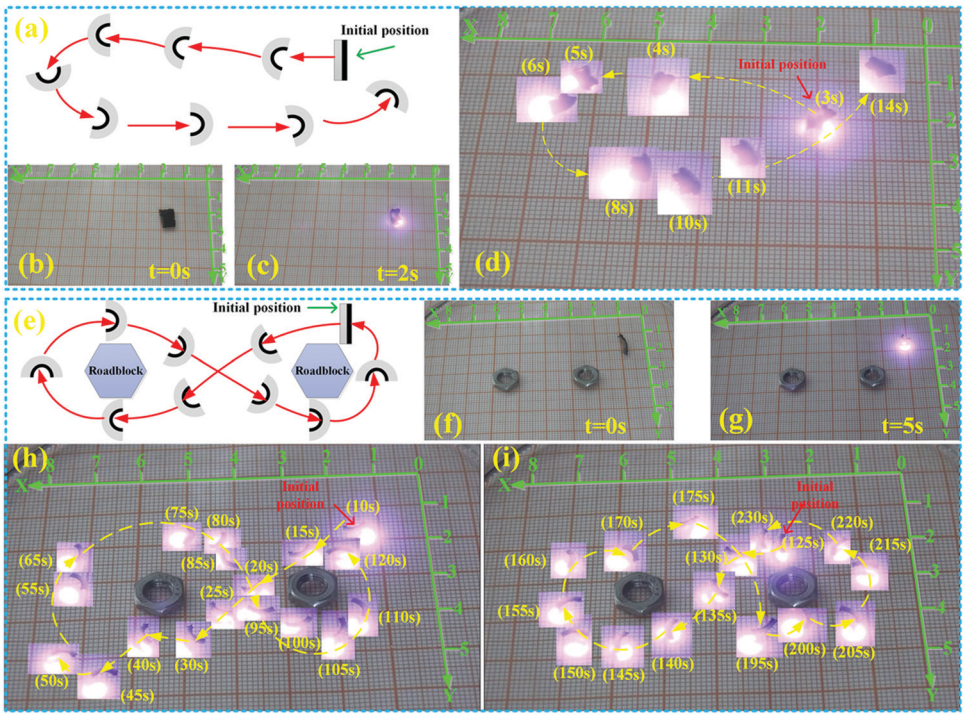

Fig. 7 The controllable movement process of gradient intelligent hydrogels with different NFC contents. (a) Motion trail schematic diagram of the "forward" and "turn" processes of NFC0, (b) initial position of NFC0, (c) flotage state of NFC0, (d) movement process of NFC0 with a power density of 31.1 W cm^{-2}, (e) motion trail schematic diagram of the "8" obstacle avoidance movement of NFC2, (f) initial state, (g) flotage state, (h) the first obstacle avoidance movement with a power density of 31.1 W cm^{-2}, and (i) the second obstacle avoidance movement with a power density of 31.1 W cm^{-2}.

shows the "forward" and "turning" movement processes of the NFC0 gradient intelligent hydrogel under an NIR power density of 31.1 W cm^{-2}. A coordinate system was built, as shown in Fig. 7(a), which was convenient for the analysis of the movement process. Layer 4 and Layer 1 were defined as the front and back of the NFC0 hydrogel, respectively. Also, the right and left parts of the NFC0 hydrogel were also defined. Under continuous NIR irradiation, the volume of the fully swollen NFC0 hydrogel shrank and it floated on the water surface, as shown in Fig. 7(b). The initial position of the NFC0 hydrogel was (2, 2) as shown in Fig. 7(c). When the laser irradiated the middle position of the back (Fig. 7(d)), the sample went through (5, 1) and (6.2, 1) and moved forward along the positive direction of the X axis. When the laser moved from the middle position to right position of the back, the NFC0 hydrogel turned left from (6.5, 1.7) in the negative direction of the X axis. When the left position of the back was irradiated, the NFC0 hydrogel turned right from (5, 3.3) to (4.2, 3.6). By changing the irradiation position from the left to the middle, the NFC0 hydrogel moved forward to (0.8, 0.5). The NFC0 intelligent hydrogel had controllable movement properties by changing the irradiation positions (see Movie S7, ESI†), which gave the efficient, controllable, continuous "forward" and "turn" movements.

Based on the "forward" and "turn" movement of the NFC0 intelligent hydrogel, the "8" obstacle avoidance movement of the NFC2 intelligent hydrogel was designed to verify the corresponding functional property. Fig. 7(e)–(i) show the schematic diagram of the obstacle avoidance movement. A coordinate system was also built to mark the movement positions of the NFC2 hydrogel. The bottom and top parts of NFC2 hydrogel were defined as the front and back, respectively, in Fig. 7(f). Together with the direction of the movement of the NFC2 hydrogel, the right and left parts were also defined. Under NIR irradiation, the NFC2 hydrogel shrank and floated on the water surface, as shown in Fig. 7(g). The initial position was (1.5, 1.7). The NFC2 hydrogel can move forward, turn right and turn left by irradiating the middle, left and right positions of the back, respectively. After irradiation for 35 s, the NFC2 hydrogel went through (2.6, 2.5), (3.6, 3.3), (4.2, 3.9), (4.8, 4.6), (5.8, 4.5) and reached (6.5, 5.3). By irradiating the left position of the back, the NFC2 hydrogel turned right to (7.2, 2.3). After changing movement direction, the NFC2 hydrogel went through (5, 1.8) and reached (1.9, 4.5). After turning left to (1.7, 2.3), the NFC2 hydrogel finished the first "8" obstacle avoidance movement, as shown in Fig. 7(h). In Fig. 7(i), the NFC2 hydrogel went from (2.7, 2) to (3, 2) in 105 s and finished the second "8" obstacle avoidance movement after 230 s. The movement trails of the two "8" obstacle avoidance movements were not completely coincident and this was attributed to the manual operation of NIR. However, the highly controllable "8" obstacle avoidance movement was repeatable (see Movie S8, ESI†). Based on the "forward" and "turn" movements, the NFC reinforced gradient intelligent hydrogels showed the functional property of a controllable, repeatable and efficient obstacle avoidance movement, which was the combination of mechanical property, intelligent property and functional property.

Analysis of the self-driven mechanisms

Based on the infiltration method of GO, the NFC reinforced gradient intelligent hydrogels had relatively high mechanical strength and multiple self-driven deformations and movements including bending deformation, curling deformation, switching movement and obstacle avoidance movement. Based on the effective regulation of Young's modulus, the NFC content was the important material parameter for the self-driven functional properties. The NFC intelligent hydrogels with a high Young's modulus exhibited a relatively low self-driven response rate and efficiency. The NIR power density and irradiation pattern were the important control parameters for the self-driven functional properties. The combination of material and control parameters achieved the deformations of ''Polymer'' and bionic drosera and movements of 90° circulatory switching, homodromous circulatory switching and ''8'' obstacle avoidance.

In order to reveal the self-driven mechanisms of NFC reinforced gradient intelligent hydrogels, the curvature variation was selected to construct the relationships of bending degree, deformation displacement, material properties and incentive intensity based on mechanical analysis. As shown in Fig. S9 (ESI†), the assumed conditions were that the layers in the bilayer simplified model of NFC reinforced gradient intelligent hydrogels were a homogeneous material and had a specific thickness. Based on the displacement equality of the bilayer model in the deformation process, the relationship of curvature, thickness ratio and Young's modulus ratio was constructed. Fig. S5 (ESI†) showed the effect of NFC content on the variation of Young's modulus. The degree of bending of the NFC reinforced intelligent hydrogels was directly influenced by the variation of the curvature values. Under the NIR irradiation, the curvature values of the intelligent hydrogels were increased and ended at the upper limit value. By using different infiltration positions, the specific letter shapes of the word ''Polymer'' were achieved. Curling deformation was induced by the bending deformation. By constructing the relationship between curvature and displacement, the displacement values of NFC reinforced gradient intelligent hydrogels were changed continuously on the basis of the NIR irradiation pattern shown in Fig. 5. In order to investigate the self-driven mechanism of movements shown in Fig. 6 and 7, a model of an elastic sheet without stress was built and is shown in Fig. S12, ESI.† The Föppl–von Kármán elastic theory was used to analyse the plane bending phenomenon. Relationships between the curvature of the NFC reinforced intelligent hydrogels on the y axis and x axis and the NIR power density were constructed. The Rayleigh–Ritz method was used to satisfy the energy conservation and indicated the two conditions of longitudinal curvature and transverse curvature of intelligent hydrogels, as shown in Fig. S13 (ESI†). With the increase of power density, the relationship between longitudinal curvature and transverse curvature changed from equality to inverse, which achieved the 90° circulatory switching and homodromous circulatory switching by affecting the torque values of the hydrogels on x axis and y axis, respectively. The driving force of the NFC2 intelligent hydrogels in the obstacle avoidance movement process was directly affected by the material properties, irradiation time and NIR power density. The material distribution homogeneity and irradiation position stability changed the movement direction of NFC2 intelligent hydrogel. The irradiation distance and position were not constant, leading to the different obstacle avoidance movement tracks in Fig. 7 (ESI†) and this was attributed to the effect of the manual control of NIR.

As an effective reinforcement, the NFC enhanced mechanical strength, maintained the high response rate and enriched the self-driven patterns of the gradient intelligent hydrogels, which effectively solved the bottleneck of the combination of excellent mechanical, intelligence and functional properties of the intelligent hydrogels.

Conclusion

The NFC enhanced the crosslinking density of gradient intelligent hydrogels and reduced the gradient structure, and this was attributed to the effect of the hydroxide radical on the addition reaction and dehydration synthesis of PNIPAm–4HBA–OH. In addition to the relatively high mechanical strength, the NFC reinforced gradient intelligent hydrogels had a high swelling/deswelling rate. With the increase of NFC content from 1 mg mL^{-1} to 3 mg mL^{-1}, the Young's modulus increased first and then decreased, which was the important material parameter for the variation of NIR response rate. The hydrogel with 2 mg mL^{-1} NFC exhibited the highest Young's modulus and the steadiest intelligent response process. Increasing the NIR power density effectively improved the response rate of hydrogels within certain limits. The NFC reinforced gradient intelligent hydrogels achieved the combination of mechanical property, intelligence property and functional property. Under the stimulation of NIR, the hydrogels exhibited excellent self-driven deformations and movements including bending deformation, curling deformation, switching movement and an obstacle avoidance movement. Based on mechanical analysis, the curvature variation was selected to construct its relationships with bending degree, deformation displacement, material properties and incentive intensity, thus, effectively revealing the self-driven mechanisms. The NFC reinforced gradient intelligent hydrogels had characteristics of high mechanical strength, high response rate, multiple intelligent responses and multiform deformation patterns, which provided a new candidate material for the applications of intelligent hydrogels in soft robot, drug delivery and intelligent sensing.

Experimental

Materials

N-Isopropylacrylamide (NIPAm, Aladdin, Shanghai, China, 2% stabilizer), 4-hydroxybutyl acrylate (4HBA, J&K Scientific Ltd, Beijing, China) and non-carboxylated nanofibrillated cellulose (NFC, Guilin Qihong Technology Co., Ltd, Guilin, China) were

Table 1 Compositions of the gradient structure intelligent hydrogels

Sample	NFC (mg)	NIPAm (g)	APS (mg)	4HBA (μL)	H_2O (mL)
NFC0	0	1	10	210	10
NFC1	10	1	10	210	10
NFC2	20	1	10	210	10
NFC3	30	1	10	210	10

selected as the monomer, crosslinking agent and reinforcement, respectively. Ammonium persulfate (APS, $(NH_4)_2S_2O_8$, Sinopharm Chemical Reagent Co., Ltd, Shanghai, China) was the initiator and graphene oxide (GO, Suzhou Hengqiu Graphene Technology Co., Ltd, Suzhou, China) was the photothermal conversion agent and both chemicals were used as received. Pure water (resistivity $\geq$18.2 MΩ cm) was obtained by deionization and filtration.

Preparation of the NFC reinforced intelligent hydrogels

Before the preparation of the NFC reinforced intelligent hydrogels, the pure water was degassed in a continuous nitrogen-saturated atmosphere for 2 h. In an iced water bath, a specific weight of NFC was added into 10 mL of pure water and stirred for 0.5 h with a magnetic stirrer (Model DF-101S, Changchun Jiyu Technology Equipment Co., Ltd, China). Then, 1 g of NIPAm and 10 mg of APS were added into the NFC aqueous solution and stirred for 1 h. After addition of 210 μL of 4HBA and stirring for 5 min, the reaction mixture was filtered into a 200 mL reaction kettle and heated to 190 °C for 5 h in a circulated air drying oven (Model 101A-1E, Shanghai Laboratory Instrument Works Co., Ltd, Shanghai, China) to complete the synthesis of the NFC containing intelligent hydrogels. The compositions of gradient structure intelligent hydrogels are given in Table 1. Based on the NFC content, the prepared hydrogels were designated as NFC0, NFC1, NFC2 and NFC3.

Microstructure

In order to investigate the effect of NFC content on the microstructure variation of the gradient intelligent hydrogels, the cross sections of the freeze-dried (LGJ-10C, Beijing Four Ring Scientific Instrument Factory Co., Ltd, Beijing, China) hydrogels were observed using FE-SEM (Model XL30, FEI, OR, USA).

Infrared spectroscopy and differential scanning calorimetry

The Fourier transform infrared spectra (FT-IR, IRAffinity-1 FT-IR spectrometer, Shimadzu, Kyoto, Japan) characteristics of the hydrogels were determined. The wavenumber range was 500–4000 cm^{-1}. Differential scanning calorimetry (DSC) (Model DSC25-RCS90, TA Instruments, USA) was used to determine the volume phase transition temperature of the hydrogels. The temperature variation range was from 10 to 60 °C with a heating rate of 20 °C min^{-1} in a nitrogen atmosphere.

Young's modulus and near infrared laser response rate

The effect of NFC variation on the Young's modulus of the hydrogels was obtained using the ultrasound image diagnostic apparatus (Aixplorer, Supersonic Imagine, Aix-en-Provence, France) with an SL15-4 probe. In order to quantify the effect of NFC variation on the NIR laser response rate of intelligent hydrogels, the entire infiltrated hydrogel strips with dimensions of 30 mm × 3 mm × 2 mm (length × width × thickness) were immersed in pure water. The powers of NIR used were 2.4 W, 7.1 W, 11.8 W and 16.5 W. Based on a laser spot diameter of 7 mm, the power densities were 6.32 W cm^{-2}, 18.7 W cm^{-2}, 31.1 W cm^{-2} and 43.4 W cm^{-2}, respectively. The NIR irradiation was on the middle part of the hydrogel strip from a distance of 50 cm. The NIR response process was recorded on a high-speed camera (dlmax HD, PCO Imaging Asia Ltd. Pte, Germany). The bending angle was used to represent the response rate.

Bending deformation, curling deformation, folding deformation, switching movement and forward/turn movement were selected to realize the multiple self-driven patterns of the hydrogel actuators.

Preparation of "Polymer"

The combination of monodirectional and bidirectional bending deformations of the NFC0 gradient intelligent hydrogel can cause the deformation of "Polymer" by locality infiltration. Layer 4 and the adjacent part of Layer 3 was used to realize the monodirectional deformation of "P", "o", "l" and "e". Layer 3 was used to realize the bidirectional deformation of "y", "m" and "r". The locality infiltration depth was half of the sample thickness. The power density of NIR was 18.7 W cm^{-2}.

Preparation of bionic drosera

After entire infiltration of the GO had been achieved, the NFC reinforced gradient intelligent hydrogels with dimensions of 30 mm × 3 mm × 2 mm (length × width × thickness) were used to prepare the bionic drosera. The left part of hydrogel strip was fixed. The hydrogel strips were irradiated by NIR with 18.7 W cm^{-2} from right part to left part.

The 90° bending and syntropy cyclic switching movements

In order to investigate the effect of NIR power density on the movement patterns of hydrogels, power densities of 6.32 W cm^{-2} and 18.7 W cm^{-2} were adopted to irradiate the NFC2 hydrogels with dimensions of 10 mm × 1 mm × 2 mm (length × width × thickness). After the intermittent and cyclic irradiation, the movement patterns were recorded with a digital camera.

"8" obstacle avoidance movement

Under a power density of 31.1 W cm^{-2}, the NFC0 hydrogel with dimensions of 10 mm × 3 mm × 5 mm (length × width × thickness) and the NFC2 hydrogel with dimensions of 10 mm × 1 mm × 2 mm (length × width × thickness) were used to cause the "forward" and "turn" movements by changing the continuous irradiation to different parts of the hydrogels. Based on the movement property, two nuts were used as an obstacle to design the "8" obstacle avoidance movement. Mathematical and mechanical models were built to analyse and reveal the self-driven mechanisms of intelligent actuators.

Conflicts of interest

The authors declare no competing financial interest.

Acknowledgements

This work was supported by the Project of National Key Research and Development Program of China (Grant No. 2018YFC0703300, 2018YFB1105100 and 2018YFA2001300), the National Natural Science Foundation of China (Grant No. 51822504, 5167050531, 91948302, 91848204), the Key Scientific and Technological Project of Jilin Province (20180201051GX), the Program for JLU Science and Technology Innovative Research Team (2017TD-04), the Joint Fund of Ministry of Education for Equipment Pre-research (2018G944J00084) and the China Postdoctoral Science Foundation (Grant No. 2019M661204, 2020M670845).

Notes and references

1 S. Y. Zheng, Y. Y. Shen, F. B. Zhu, J. Yin, J. Qian, J. Z. Fu, Z. L. Wu and Q. Zheng, *Adv. Funct. Mater.*, 2018, **28**, 1803366.
2 H. Q. Shao, S. Z. Wei, X. Jiang, D. P. Holmes and T. K. Ghosh, *Adv. Funct. Mater.*, 2018, **28**, 1802999.
3 A. N. Hakan, A. K. Lee and K. Yum, *Nat. Commun.*, 2018, **9**, 3705–3716.
4 X. Q. Wang, C. F. Tan, K. Chan, X. Lu, L. L. Zhu, S. W. Kim and G. W. Ho, *Nat. Commun.*, 2018, **9**, 3438–3448.
5 M. T. Tolley, R. F. Shepherd, B. Mosadegh, K. C. Galloway, M. Wehner, M. Karpelson, R. J. Wood and G. M. Whitesides, *Soft Robot.*, 2014, **1**, 213–223.
6 S. Seok, C. Denizel, K. J. Cho, R. J. Wood, D. Rus and S. Kim, *IEEE ASME Trans. Mechatron.*, 2013, **18**, 1485–1497.
7 W. N. Chen, M. M. Sun, X. J. Fan and H. Xie, *Appl. Mater. Today*, 2020, **19**, 100583.
8 D. Rus and M. T. Tolley, *Nature*, 2015, **521**, 467–475.
9 T. Mirfakhrai, J. D. W. Madden and R. H. Baughman, *Mater. Today*, 2007, **10**, 30–38.
10 F. Rosso, G. Marino, A. Giordano, M. Barbarisi, D. Parmeggiani and A. Barbarisi, *J. Cell. Physiol.*, 2005, **203**, 465–470.
11 D. Morales, E. Palleau, M. D. Dickey and O. D. Velev, *Soft Matter*, 2014, **10**, 1337–1348.
12 A. F. Kanaan, A. P. Piedade, H. C. de Sousa and A. M. A. Dias, *Appl. Mater. Today*, 2020, **20**, 100711.
13 S. Wang, Y. Gao, A. Wei, P. Xiao, Y. Liang, W. Lu, C. Chen, C. Zhang, G. Yang, H. M. Yao and T. Chen, *Nat. Commun.*, 2020, **11**, 4359–4671.
14 X. Q. Wang, K. H. Chan, Y. Cheng, T. P. Ding, T. T. Li, S. Achavananthadith, S. Ahmet, J. S. Ho and G. W. Ho, *Adv. Mater.*, 2020, **32**, 2000351.
15 J. Loomis, P. Xu and B. Panchapakesan, *Nanotechnology*, 2013, **24**, 185703.
16 Y. Hwang, S. Kang, S. Cha and S. Choi, *Sens. Actuators, A*, 2016, **249**, 163–171.
17 T. J. Kang, K. H. Hong and H. Jeong, *Polym. Eng. Sci.*, 2015, **55**, 729–734.
18 J. Shintake, S. Rosset, B. Schubert, D. Floreano and H. Shea, *Adv. Mater.*, 2016, **28**, 231–238.
19 F. Lancia, A. Ryabchun, A. D. Nguindjel, S. Kwangmettatam and N. Katsonis, *Nat. Commun.*, 2019, **10**, 4819–4827.
20 C. Lin, J. X. Lv, Y. S. Li, F. H. Zhang, J. R. Li, Y. J. Liu, L. W. Liu and J. S. Leng, *Adv. Funct. Mater.*, 2019, 1906569.
21 L. Ionov, *Adv. Funct. Mater.*, 2013, **23**, 4555–4570.
22 H. Lei, L. Dong, Y. Li, J. S. Zhang, H. Y. Chen, J. H. Wu, Y. Zhang, Q. Y. Fan, B. Xue, M. Qin, B. Chen, Y. Cao and W. Wang, *Nat. Commun.*, 2020, **11**, 4032–4042.
23 M. T. Li, X. Wang, B. Dong and M. Sitti, *Nat. Commun.*, 2020, **11**, 3988–3998.
24 R. C. Luo, J. Wu, N. D. Dinh and C. H. Chen, *Adv. Funct. Mater.*, 2015, **25**, 7272–7279.
25 C. Yao, Z. Liu, C. Yang, W. Wang, X. J. Ju, R. Xie and L. Y. Chu, *Adv. Funct. Mater.*, 2015, **25**, 2980–2991.
26 D. Han, C. Farino, C. Yang, T. Scott, D. Browe, W. Choi, J. W. Freeman and H. Lee, *ACS Appl. Mater. Interfaces*, 2018, **10**, 17512–17518.
27 D. Han, C. Farino, C. Yang, T. Scott, D. Browe, W. Choi, J. W. Freeman and H. Lee, *Nature*, 2018, **554**, 81–86.
28 Y. Y. Yang, Y. T. Liu and Y. J. Shen, *Adv. Funct. Mater.*, 2020, **30**, 1910172.
29 Y. Cheng, K. Hoe, C. Q. Wang, T. P. Ding, T. T. Li, X. Lu and G. W. Ho, *ACS Nano*, 2019, **13**, 13176.
30 E. Z. Zhang, T. Wang, L. Zhao, W. X. Sun, X. X. Liu and Z. Tong, *ACS Appl. Mater. Interfaces*, 2014, **6**, 22855–22861.
31 Y. Wang, J. Y. Zhang, C. B. Qiu, J. B. Li, Z. X. Cao, C. S. Ma, J. Zheng and G. S. Huang, *Carbohydr. Polym.*, 2018, **196**, 82–91.
32 X. F. Wan, C. B. Guo, Y. Liu, X. S. Chai, Y. M. Li and G. X. Chen, *Chemosphere*, 2018, **194**, 297–305.
33 Q. Zhao, Y. H. Liang, L. Ren, Z. L. Yu, Z. H. Zhang and L. Q. Ren, *Nano Energy*, 2018, **51**, 621–631.
34 J. Li, Z. Y. Xu, W. B. Wu, Y. Jing, H. Q. Dai and G. G. Fang, *Colloid. Surface. A*, 2018, **538**, 474–480.
35 Q. Zhao, Y. H. Liang, L. Ren, Z. L. Yu, Z. H. Zhang, F. Qiu and L. Q. Ren, *J. Mater. Chem. B*, 2018, **6**, 1260–1272.